IMPACT OF SCATTERING MODEL ON DISDROMETER DERIVED ATTENUATION SCALING

Michael Zemba, NASA Glenn Research Center, 21000 Brookpark Rd. MS 54-1, Cleveland, OH 44135, +1 216-433-5357, michael.j.zemba@nasa.gov

Lorenzo Luini, Politecnico di Milano, Via Ponzio 34/5, 20133 - Milano, +39 02-23993693, lorenzo.luini@polimi.it

James Nessel, NASA Glenn Research Center, 21000 Brookpark Rd. MS 54-1, Cleveland, OH 44135, +1 216-433-2546, james.a.nessel@nasa.gov

Carlo Riva, Politecnico di Milano, Via Ponzio 34/5, 20133 - Milano, +39 02-23993659, carlo.riva@polimi.it

Abstract

NASA Glenn Research Center (GRC), the Air Force Research Laboratory (AFRL), and the Politecnico di Milano (POLIMI) are currently entering the third year of a joint propagation study in Milan, Italy utilizing the 20 and 40 GHz beacons of the Alphasat TDP#5 Aldo Paraboni scientific payload. The Ka- and Q-band beacon receivers were installed at the POLIMI campus in June of 2014 and provide direct measurements of signal attenuation at each frequency. Collocated weather instrumentation provides concurrent measurement of atmospheric conditions at the receiver; included among these weather instruments is a Thies Clima Laser Precipitation Monitor (optical disdrometer) which records droplet size distributions (DSD) and droplet velocity distributions (DVD) during precipitation events. This information can be used to derive the specific attenuation at frequencies of interest and thereby scale measured attenuation data from one frequency to another. Given the ability to both predict the 40 GHz attenuation from the disdrometer and the 20 GHz timeseries as well as to directly measure the 40 GHz attenuation with the beacon receiver, the Milan terminal is uniquely able to assess these scaling techniques and refine the methods used to infer attenuation from disdrometer data.

In order to derive specific attenuation from the DSD, the forward scattering coefficient must be computed. In previous work, this has been done using the Mie scattering model, however, this assumes a spherical droplet shape. The primary goal of this analysis is to assess the impact of the scattering model and droplet shape on disdrometer derived attenuation predictions by comparing the use of the Mie scattering model to the use of the T-matrix method, which does not assume a spherical droplet. In particular, this paper will investigate the impact of these two scattering approaches on the error of the resulting predictions as well as on the relationship between prediction error and rain rate.

I. Introduction

Since June of 2014, NASA Glenn Research Center (GRC), the Air Force Research Laboratory (AFRL), and the Politecnico di Milano (POLIMI) have jointly operated a measurement campaign in Milan, Italy to characterize atmospheric propagation phenomena at Ka and Q-band using the Alphasat TDP#5 Aldo Paraboni Q/V-band payload. The experiment is installed at the POLIMI campus on the roof of the Dipartimento di Elettronica, Informazione e Bioingegneria (DEIB) building, and consists of two receivers monitoring the 19.701 GHz and 39.402 GHz Alphasat beacons along with a host of collocated meteorological instrumentation to record ground level weather conditions.

The Ka- and Q-band beacon receivers (Fig. 1a) provide an 8 Hz measurement of link power, from which the excess attenuation and scintillation at each frequency can be derived. The weather instrumentation provides measurements of temperature, pressure, humidity, wind speed and wind direction, as well as rain rate and rain accumulation via a tipping bucket. A Thies Clima laser disdrometer (Fig. 1b) yields droplet size and velocity distributions (DSD, DVD), from which an optical measurement of rain rate and accumulation can also be calculated. More importantly for this analysis, the droplet size distribution can be used to calculate the expected specific attenuation at each frequency; by doing so, an instantaneous scaling factor (ISF) can then be derived

Figure 1. The Ka- and Q-band beacon receivers (left) and the Thies Clima optical disdrometer (right), installed in April 2014 at the POLIMI campus in Milan, Italy.

to translate the measured 20 GHz attenuation data to an expected 40 GHz attenuation timeseries. Given that the 40 GHz attenuation is also being directly measured by the beacon receiver, the prediction can be compared to the measurement in order to characterize the ISF in terms of accuracy and statistical variation.

Previous publications along these lines have investigated the statistics of the ISF including the probability distribution function, seasonal variations, and the prediction error as a function of attenuation level [1 - 2]. However, these prior analyses have always used the Mie scattering model in the computation of the specific attenuation. This is a widely accepted model, but it assumes a spherical droplet shape, while rain droplets tend toward a more oblate spheroid shape for larger diameter particles [3]. This paper thus turns to the scattering model to investigate the impact of using a model that does not assume a spherical shape – namely, the T-Matrix method [4]. This approach allows for the calculation of the extinction coefficient assuming oblate spheroids of varying axial ratio. This analysis therefore aims to assess the accuracy of these two scattering models as compared to the measured attenuation data and quantify the necessity of presuming non-spherical droplets.

II. Experiment Design

Ka/Q-Band Beacon Receivers

The Alphasat beacon receivers were developed and tested at NASA Glenn Research Center in Cleveland, Ohio prior to their deployment for the measurement campaign. The receivers utilize a 1.2m Ka-band and a 0.6m Q-band Cassegrain reflector, each with a beamwidth of 0.9°. Active tracking of the beacons is employed with electronic positioners that update the pointing once per minute with a resolution of 0.01°, eliminating the need to compensate for satellite motion in the attenuation data.

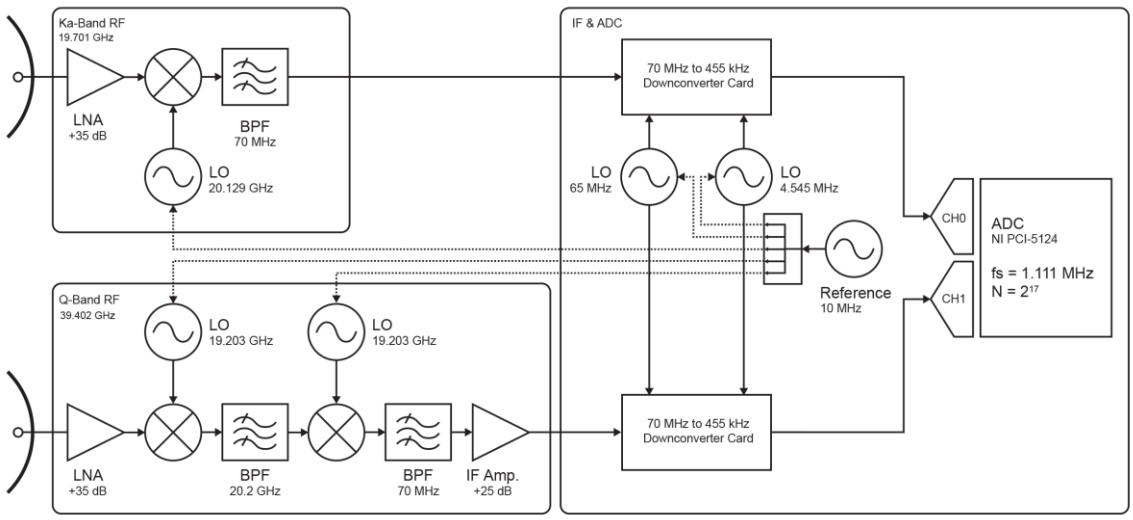

Figure 2. Block diagram of the Ka- and Q-band beacon receiver system.

Both signals are first amplified via a 35 dB low-noise amplifier and subsequently downconverted to 70 MHz immediately at the feed in a climate-controlled enclosure. Downconversion to 70 MHz occurs in one stage on the Ka-band side, and in two stages on the Q-band side. The LNAs and other RF electronics (oscillators, mixers, etc.) are all thermally controlled to within ±0.1°C. Both signals are then fed into a common IF stage (thermally controlled to within ±1.0°C) and further downconverted to 455 kHz, as shown in the block diagram of Fig. 2. All oscillators are referenced to a common 10 MHz ultra-stable reference oscillator. After the 455 kHz downconversion, the resulting signals are digitized with an NI PCI-5124 ADC and processed using a novel frequency estimation technique [5] to record the observed frequency and power level of each channel. Data is recorded at a measurement rate of 8 Hz, and the total achieved dynamic range of the receivers is 40 dB. The design and validation of the receivers is further detailed in [6].

Thies Clima Disdrometer

The Thies Clima Disdrometer is located approximately 6 meters from the beacon receivers on the DEIB rooftop (pictured in Fig. 1, right) with a wind shield around the instrument to reduce wind-related inaccuracies. The disdrometer derives a distribution of particle diameters and velocities once per minute based on the magnitude and duration of fades recorded in a 4560 mm^2 measurement area using a 750 nm infrared laser. Particles are classified into spectra of 22 diameter bins from 0.125 mm to 8 mm and 20 velocity bins from 0 to 10 m/s [7]. Using on-board processing, the type and intensity of precipitation is also classified (rain, snow, hail, etc.).

III. Data Analysis

Scattering Cross Section

The extinction cross section (the sum of the absorption and scattering components) was calculated twice for a given drop size distribution; once using the spherical Mie scattering model as in [3], and once using the non-spherical T-matrix method as in [4]. Given that non-spherical particles are not symmetric with regards to polarization, the T-matrix method produces a horizontal and vertical polarization component of the extinction cross section based on the orientation and dimensions of the particle. The Alphasat beacon is linearly polarized with an orientation of 45° so, for this analysis, the horizontal and vertical results were combined to yield the corresponding 45° component. An incident angle of 56° was used, given the average elevation look angle of 34° in Milan.

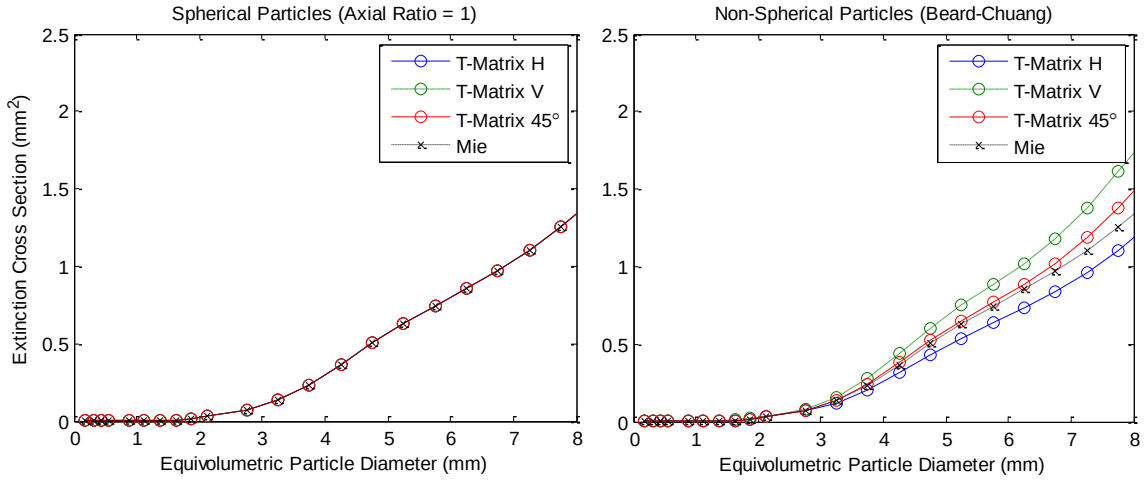

Figure 3. The extinction cross section as a function of particle diameter, with both models in agreement for spherical particles (a), and with deviation for large non-spherical particles (b).

Fig. 3 compares the extinction cross sections produced by each model as a function of the equivolumetric particle diameter. On the left, the T-matrix method is configured for an axial ratio of 1 (spherical particles), resulting in an output that matches the Mie model identically in all three cases (horizontal, vertical, and 45°) for all observed particle diameters. On the right, the T-matrix is configured for non-spherical particles utilizing the Beard-Chuang model to calculate the axial ratio of an oblate spheroid rain droplet as a function of equivolumetric diameter [8]. In this case, the two scattering models remain in agreement for particles below approximately 3 mm in diameter where the axial ratio is close to unity, but begin to diverge for larger particles. The horizontal and vertical polarizations deviate the most from the spherical Mie model, while the 45° polarization falls between the two extremes and is more in line with the spherical Mie model but still diverges for larger diameter particles.

Instantaneous Scaling Factor

The instantaneous scaling factor is derived from the disdrometer data by using the DSD to calculate the specific attenuation (γ) at both 20 GHz and 40 GHz. The resulting scaling factor, γ_{40} / γ_{20}, is then used to scale the measured 20 GHz timeseries attenuation data to 40 GHz and compare with the measured data taken at 40 GHz. Computation of the specific attenuation (γ) for a given drop density distribution N(D) at a particular frequency is a function of the wavelength λ and the forward scattering coefficient Re{S(0)} and can be calculated as in [9]:

$$\gamma = 4.343 \times 10^3 \frac{\lambda^2}{\pi} \sum Re\{S(0)\} N(D) \Delta D \qquad (1)$$

where ΔD is the drop size interval (in mm). For the purposes of this investigation into the scattering model, the forward scattering coefficient is calculated both by using the Mie model [3], assuming a spherical droplet shape, and the T-matrix model [4], assuming an axial ratio as defined by the Beard-Chuang model [8]. Computation of specific attenuation, as well as the calculation of the drop density distribution from the binned DSD data, are further detailed in [10 – 12, 15].

Isolation of Rain Events

The data used in this analysis spans two years from August 2014 through July 2016 and was processed to isolate applicable rain events from non-rainy and anomalous data. Rain events were omitted if the disdrometer was not operational, if the receivers were not operational, or if rain occurred along the path but was not measured over the receivers by the disdrometer.

For each precipitation event, the measured attenuation level before and after the event was averaged and subtracted from the attenuation time series in order to isolate the excess attenuation due to rain, though this approach may still be biased by alternate sources of attenuation. Instances where this was readily apparent were removed by inspection (primarily slow-varying, high attenuation consistent with snow or water on the feed/reflector). Rainy periods were defined as any 1 minute period where the disdrometer observed more than 5 precipitating particles (roughly 0.03 mm/hr depending on particle class), and days were included in the statistical analysis if they included at least 10 minutes/samples exceeding this level of activity. Altogether, over the two years of observations, 1225 hours of rain events were isolated across 261 days containing rain.

IV. Results

The resulting performance of the two scattering models was considered both in terms of the predicted attenuation on an event-by-event basis, as well as on a longer statistical basis over the full two years of observation from August 2014 through July 2016.

Timeseries Examples

Three timeseries examples are presented in Fig. 4a – c, plotting the attenuation measured at 20 GHz (blue) and 40 GHz (green) alongside the attenuation predicted at 40 GHz by scaling the 20 GHz data with the ISF. The predictions of both the Mie scattering model (red) and the T-matrix scattering model (black) are shown, generally in very close agreement with one another as well as with the measured attenuation. Fig. 4a presents an example of a short, strong rain event (90 mm/hr) in April 2016 with lighter rain (3 mm/hr) earlier in the day, while Fig. 4b shows a light event (8 mm/hr) lasting the majority of the day in April 2015. Lastly, Fig. 4c presents a moderate event (18 mm/hr) from May 2016.

In Fig. 4d – f, each example rain event is characterized in terms of the change in the error of the predicted attenuation between the Mie model and the T-matrix model. This value is calculated by comparing the predicted attenuation to the measured attenuation and calculating an absolute error for each the Mie and T-matrix results, then taking the difference between the two absolute prediction errors. The difference is taken such that a positive difference implies a smaller absolute error in the T-matrix estimate, and a negative difference implies a smaller absolute error in the Mie estimate. In Fig 4d, the lighter rain of the event corresponds to an equivalence between the two models -- for attenuation below 10 dB, the difference in the

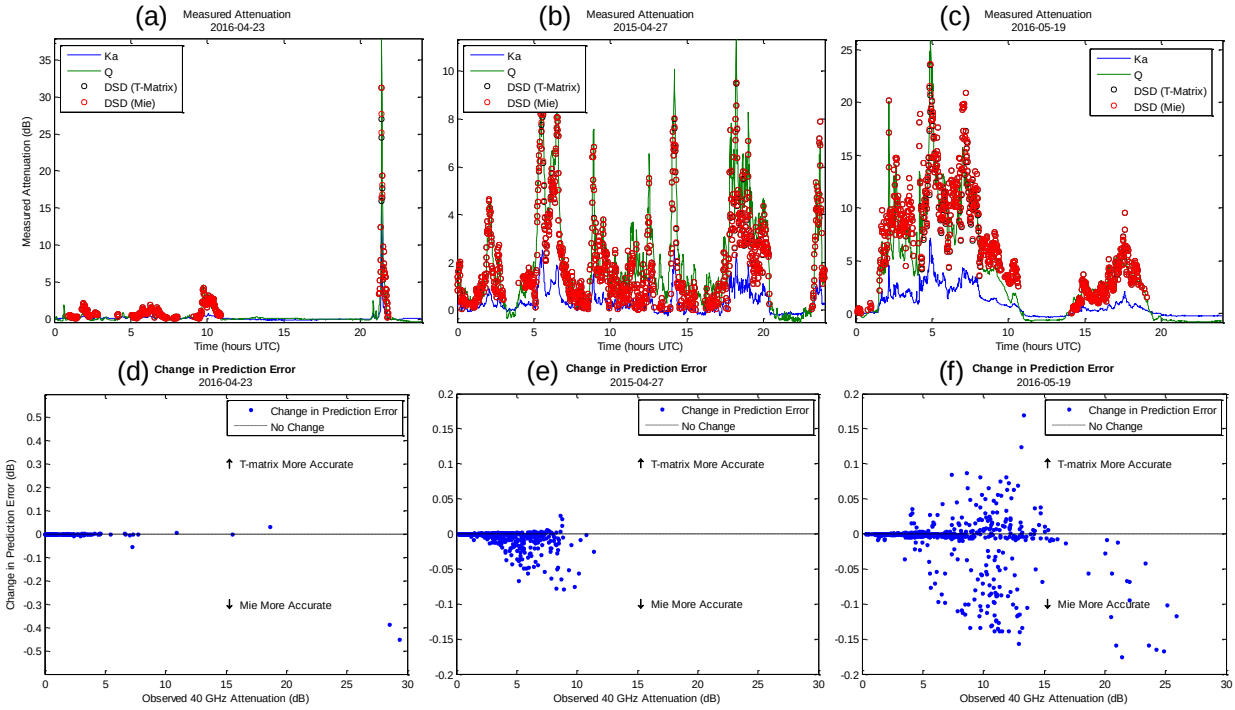

Figure 4. (a – c) example timeseries data comparing the measured attenuation at 20 GHz (blue) and 40 GHz (green) is plotted with the attenuation predicted by the ISF using the Mie model (red) and T-matrix model (black). (d – f) the associated change in absolute prediction error between the Mie and T-Matrix models is shown for each example.

prediction errors is negligible. During the few minutes at the height of the heavy event there is increasing difference between the predictions, with up to 0.5 dB better prediction from the Mie model. In Fig. 4e, most of the event is below 10 dB of observed attenuation, and while the difference in prediction error is often near zero, there is a strong bias toward the Mie providing a better prediction, up to 0.1 dB as observed attenuation increases. Lastly, in Fig. 4f, the models again remain consistent for most of the event, but at various points the T-matrix and the Mie performed better than one another in small subsets of the event – up to approximately 0.2 dB lower prediction error in both cases.

Statistical Performance

As described in Section III, rain events were isolated to cases where are least 5 particles were observed by the disdrometer in a given sampling period, and included in the following statistical analysis if 10 or more rainy minutes (not necessarily continuous) were observed throughout a given day. In Fig. 5a, the specific attenuation

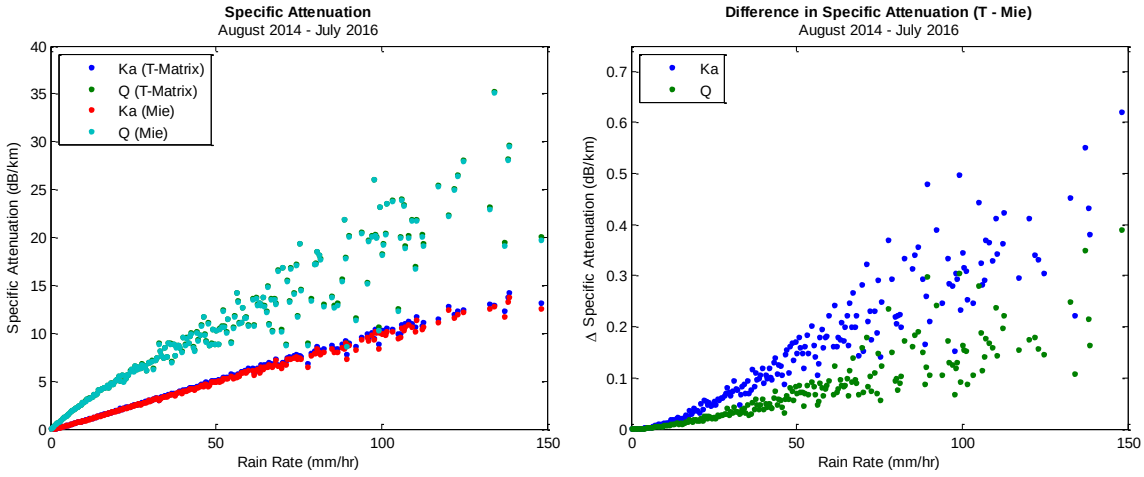

Figure 5. (a) Specific attenuation vs. rain rate over the observed two year period, averaged over bins of 0.5 mm / hr. (b) The change in specific attenuation (as a function of rain rate) from the Mie to the T-matrix model, again averaged over bins of 0.5 mm / hr.

is plotted for each frequency and for each model as a function of rain rate over the two year observation period, and averaged across rain rate bins of 0.5 mm / hr. Differences between the two models are very minor, particularly below rain rates of 50 - 75 mm/hr. In Fig. 5b, the difference between the specific attenuation predicted by the T-matrix and the Mie models is plotted versus rain rate (again, averaged over rain rate bins of 0.5 mm/hr). The difference in the specific attenuation resulting from two models was extremely low -- less than 0.01 dB / km difference for 97.6% of time that rain was measured by the disdrometer.

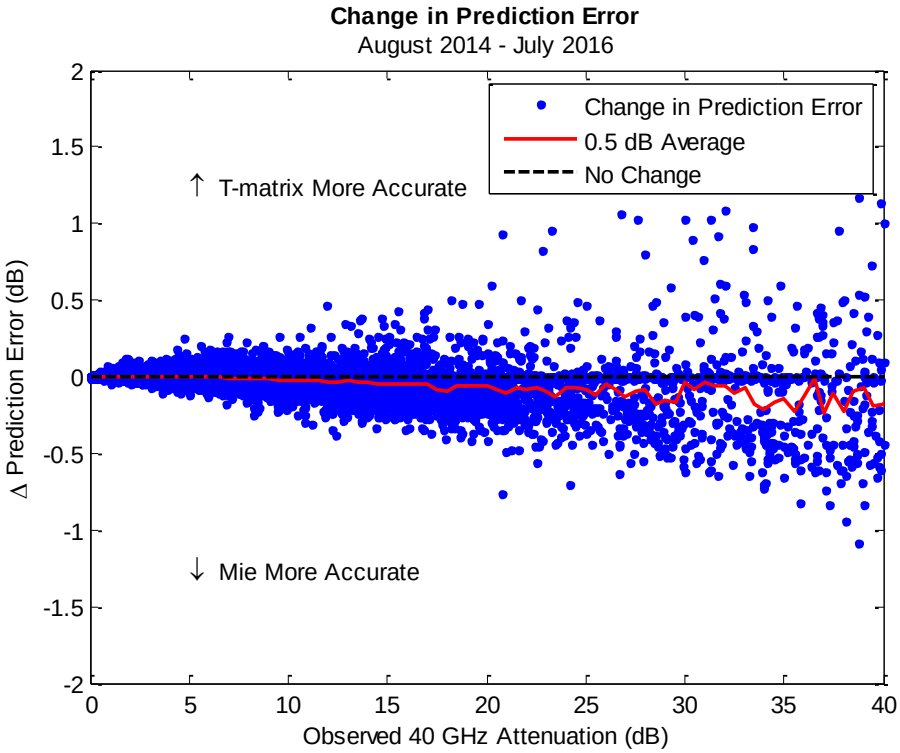

Figure 6. The change in prediction error across all two years of observations (blue) as a function of the measured 40 GHz attenuation, also plotted averaged over bins of 0.5 dB (red).

In Fig. 6, the change in the predicted attenuation error is plotted as a function of observed attenuation, both as a scatter plot of all observations (blue) and averaged across bins of 0.5 dB observed attenuation (red). Across all observations, the predicted attenuation was more accurate using the Mie model 41.3% of the time, and more accurate with the T-matrix model 28.0% of the time, with no measurable change in the prediction error the remaining 30.7% of the time. As shown by the average, there is a slight bias toward the Mie model being more accurate beyond 15 – 20 dB of observed attenuation. However, even in the case where one model is favorable over the other, the differences are very minor; the change in the predicted attenuation error was less than 0.1 dB for 97.2% of observations, and did not exceed 1.8 dB over the two years of observation.

V. Concluding Remarks

In many cases, particularly for low rain-rate events, there was found to be little difference between the two models (Fig. 4d), with 97.2% of observations showing less than 0.1 dB change between the errors of the two predictions, and the change never exceeding 1.8 dB. In all likelihood, this points to any error of the predicted attenuation being predominantly due to not the scattering model, but to another larger source of error in the attenuation measurement such as clouds, antenna wetting, or rain along the path.

At higher rain rates, one model does tend to be preferable but only on a specific case-by-case basis, with a bias toward the Mie model being the preferred model more frequently (Fig 4e). This may be due to the fact that the disdrometer DSD becomes less representative of conditions along the path for larger diameter DSDs, due to its small measurement area, as noted in [13]. Similar findings of small change in specific attenuation were also reported by Chen, Chu and Tzeng [14] who found a difference of 0.15 dB/km in specific attenuation at 28 GHz for a 160 mm/hr rain rate between Mie and T-Matrix predictions.

As shown in the scattering cross sections of Fig. 3b, the Mie and T-Matrix models do not significantly diverge until a droplet diameter of at least 3 mm -- and in the 45° polarization case, not until approximately 6 mm or

greater, which is rarely observed. However, there may be a larger impact for links with strictly horizontal or vertical polarizations. In this case, however, the error introduced by the scattering model or non-spherical droplet shape is ultimately likely to be less than other errors in the excess attenuation prediction, such as in the calibration of excess attenuation with respect to gaseous absorption, or error due to the disdrometer sampling area not being representative of conditions along the path.

It is possible that higher frequency links may have more contribution due to scattering and may be more susceptible to differences in the scattering model. NASA GRC and AFRL are also participating in a terrestrial link at 72 GHz and 84 GHz with a collocated disdrometer which may be a candidate for future work along these lines of study.

VI. References

[1] J. Nessel, M. Zemba, L. Luini, C. Riva, "Comparison of Instantaneous Frequency Scaling from Rain Attenuation and Optical Disdrometer Measurements at K/Q bands", 21st Ka and Broadband Communications Conference, Bologna, Italy, October 2015.

[2] M. Zemba, J. Nessel, J. Houts, L. Luini, C. Riva, "Statistical Analysis of Instantaneous Frequency Scaling Factor as Derived from Optical Disdrometer Measurements at K/Q-Bands," 10th European Conference on Antennas and Propagation, Davos, Switzerland, 2016.

[3] C. Bohren, D. Huffman, Absorption and Scattering of Light by Small Particles, Wiley, 1983.

[4] M. Mishchenko, L. Travis and A. Lacis, "Scattering, Absorption, and Emission of Light by Small Particles," Cambridge University, 2002.

[5] M. Zemba, J. Morse, J. Nessel, "Frequency Estimator Performance for a Software-based Beacon Receiver," IEEE Antennas and Propagation Symposium, July 2014, pp.1574-1575.

[6] J. Nessel, J. Morse, M. Zemba, C. Riva, L. Luini, "Preliminary Results of the NASA Beacon Receiver for the Alphasat Aldo Paraboni TDP5 Propagation Experiment," 20th Ka and Broadband Communications Conference, Salerno, Italy, October 2014.

[7] Thies Clima Laser Precipitation Monitor: Instructions for Use. Rev. 2.5. July 2011.

[8] K. Beard and C. Chuang, "A New Model for the Equilibrium Shape of Raindrops," Journal of the Atmospheric Sciences, Vol. 44, No. 11, pp. 1509 – 1524, 1987.

[9] M. Sadiku, Numerical Techniques in Electromagnetics, 2nd Ed., CRC Press, 2001.

[10] C. Bohren, D. Huffman, Absorption and Scattering of Light by Small Particles, Wiley, 1983.

[11] H.Y. Lam, J. Din, L. Luini, A. Panagopoulos, C. Capsoni, "Analysis of Raindrop Size Distribution Characteristics in Malaysia for Rain Attenuation Prediction," 2011 URSI General Assembly and Scientific Symposium, August 2011.

[12] R. Gunn, G.D. Kinzer, "The terminal velocity of fall for water droplets in stagnant air," Journal of Meteorology, Vol. 8, pp.249-253, 1949.

[13] A. Ryzhkov and D. Zmic, "Radar Polarimetry at S, C, and X Bands: Comparitive Analysis and Operational Implications," University of Oklahoma, Norman, OK, 2005.

[14] K. S. Chen, C. Y. Chu, Y. C. Tzeng, "A Semi-Empirical Model of Rain Attenuation at Ka-Band in Northern Taiwan," Progress in Electromagnetics Research M, Vol. 16, pp. 213-223, 2011.

[15] R. Gunn, G.D. Kinzer, "The terminal velocity of fall for water droplets in stagnant air," Journal of Meteorology, Vol. 8, pp.249-253, 1949.

[16] H.Y. Lam, L. Luini, J. Din, C. Capsoni, A. D. Panagopoulos, "Investigation of Rain Attenuation in Equatorial Kuala Lumpur", IEEE Antennas and Wireless Propagation Letters, vol. 11, Page(s): 1002-1005, doi: 10.1109/LAWP.2012.2214371, 2012.